Parente,P., Leguey, T., Castro, V. de, Gigl, T., Reiner, M., Hugenschmidt, C. y Pareja, R. (2015). Characterization of ion-irradiated ODS Fe–Cr alloys by doppler broadening spectroscopy using a positron beam. *Journal of Nuclear Materials*, 464 , pp. 140-146.

DOI: https://doi.org/10.1016/j.jnucmat.2015.04.033

CHARACTERIZATION OF ION-IRRADIATED ODS Fe-Cr ALLOYS BY DOPPLER BROADENING SPECTROSCOPY USING A POSITRON BEAM

P. Parente[1], T. Leguey[1], V. de Castro[1,*], T. Gigl[2], M. Reiner[2], C. Hugenschmidt[2], R. Pareja[1]

[1] Departamento de Física and IAAB. Universidad Carlos III de Madrid. 28911-Leganés, Spain

[2] FRM II and Physics Department, Technische Universität München. 85747 Garching, Germany

Abstract

The damage profile of oxide dispersion strengthened steels after single-, or simultaneous triple-ion irradiation at different conditions has been characterized using a low energy positron beam in order to provide information on microstructural changes induced by irradiation. Doppler broadening and coincident Doppler broadening measurements of the positron annihilation line have been performed on different Fe-Cr-(W,Ti) alloys reinforced with Y_2O_3, to identify the nature and stability of irradiation-induced open-volume defects and their possible association with the oxide nanoparticles. It was found that irradiation induced vacancy clusters are associated with Cr atoms. The results are of highest interest for modelling the damage induced by 14 MeV neutrons in reduced activation Fe-Cr alloys relevant for fusion devices.

Keywords: Slow positron beam, positron annihilation spectroscopy, ODS steels, nanostructured materials, ion irradiation

1. Introduction

High-chromium (9-14 wt.%) advanced ferritic/martensitic and ferritic steels are promising structural materials for future fusion reactors and generation IV fission reactors [1-3]. These steels have been developed during the last decades due to their favorable mechanical properties such as high strength and their superior resistance to radiation damage compared to austenitic steels [4-6]. Moreover, their mechanical properties can still be enhanced by a fine dispersion of nanoparticles. Yttria (Y_2O_3), as one of the most stable oxides being thermodynamically more stable than nitrides and carbides, is the typical reinforcement phase used for producing oxide dispersion strengthened (ODS) materials [7]. ODS ferritic Fe-Cr alloys appear to exhibit superior creep resistance and stability under irradiation, and meet the reduced activation criteria that will be demanded for structural materials in the future nuclear reactors [8, 9]. The study of the irradiation effect on the microstructure of these materials is object of ever growing interest and investigation because of the impact on their mechanical properties, and therefore on the efficiency and reliability of future nuclear power plants. Thus, it is crucial to understand the microstructural changes driven by irradiation to predict the degradation of structural materials under their working conditions [3, 10].

14 MeV neutrons from fusion reactions produce atom displacements by elastic collisions causing Frenkel pairs. The evolution of this primary irradiation damage changes the microstructure, produces agglomeration of vacancies and interstitials into voids and dislocation loops, and consequently degrades the mechanical properties [11]. Besides, (n,α) and (n,p) transmutation reactions generate He and H gases. Small contents of these transmutation gases can also induce deleterious effects on mechanical properties, in particular when He atoms form small bubbles decorating grain boundaries [12].

A way of simulating the combined effect of displacement damage and He and H transmutation induced by high-energy neutrons would be the simultaneous irradiation of the

material under study with Fe^{4+}, He^{+} and H^{+} ions in a triple ion beam facility. This technique allows attaining significant displacement damage along with high He and H contents in samples irradiated for short periods of time. The generated displacement damage as well as the implanted He^{+} and H^{+} ions would be confined to a region beneath the sample surface due to the short range of the implanted ions [13].

Positron annihilation spectroscopy (PAS) is a very effective technique to investigate open-volume defects in metals because they are strong traps for thermal positrons in the crystal lattice. This technique has been successfully applied to study radiation damage in the bulk of steels used in nuclear technology [14-17]. Using variable-energy positron beams it is possible to profile irradiation-induced defects in the near-surface region of ion-irradiated metallic samples [18-20]. An implanted positron after being thermalized diffuses until it annihilates with an electron of the medium producing mainly two annihilation photons of ~511 keV. The positron can annihilate in a Bloch state in the lattice or in a trapped state in an open-volume defect. The annihilation radiation conveys information about the annihilation sites of the implanted positrons. In addition to positron lifetime measurements, which provide information about the nature and size of the positron traps, Doppler broadening (DB) measurements of the annihilation radiation can reveal useful information on the chemical environment of the positron trapping sites [21]. Thus, DB and coincidence DB (CDB) measurements in Fe-Cr alloys could contribute to elucidate the nature, localization and thermal stability of the defects responsible for the swelling resistance and detrimental effects on the mechanical properties.

DB and CDB are PAS techniques based on the measurement of the Doppler shifted annihilation photons, which depends almost exclusively on the momentum distribution of the annihilation electrons since the momentum of a thermalized positron is negligible. Due to the

element-specific electron-momentum distribution, the analysis of the DB annihilation radiation can be used to investigate the presence of open-volume defects and their chemical surrounding [22]. The potential of CDB measurements for investigating the nanosized features of non-irradiated ODS steels has been demonstrated [23, 24]. However, DB or CDB techniques have not been applied to study the irradiated steels until very recently, having few published reports [25-27].

This paper reports results of CDB experiments performed on three ODS Fe-Cr alloys, and a non-ODS Fe-Cr alloy using a variable energy positron beam. Alloys containing 12% Cr have been irradiated with high-energy Fe ions at room temperature, while alloys with a Cr content of 14% have been simultaneously irradiated with a triple beam of Fe, He and H ions at high temperature (600 ºC). The results are discussed in terms of the open volume defect structure created by the irradiations and the role of the different precipitates present in the alloys as defect trapping sites.

2. Experimental

The nominal composition and type of irradiation of the studied alloys are given in Table 1. These alloys were produced by powder metallurgy. Elemental powders were mechanically alloyed under Ar or H atmosphere and consolidated by hot isostatic pressing. After consolidation, the billets of the Fe12Cr and ODS12Cr alloys were annealed at 750ºC for 4 h, and the ODS14Cr and ODS14CrWTi alloys forged at ~1100 ºC followed by annealing at 850ºC for 2 h. Details on the production process and characterization of the resulting microstructures have been reported elsewhere [28, 29]. Samples with dimensions 7×7×0.2 mm^3 were cut out and their surfaces mechanically polished to a mirror finish using a 50 nm aqueous alumina slurry.

These samples were ion irradiated using a single or triple ion beam at the JANNUS-Saclay

Facility (France). Table 2 specifies conditions for the single and triple beam irradiations. The 12Cr alloys were irradiated at room temperature with Fe^{4+} ions to a maximum dose of 10 dpa and the 14Cr alloys were simultaneously irradiated at 600ºC with Fe^{5+}, He^{+} and H^{+} to a maximum dose of 30 dpa. The conditions for the triple irradiation were selected so that the implantation profiles for the three ions attain their maximums at the same position, i.e. ~ 2.4 µm. This was the minimum depth for the Bragg peak that could be achieved, as it was limited by the minimum possible implantation energy for the H ions (500 keV). The corresponding damage profiles were calculated using SRIM2011 [30] and are depicted in Fig. 1. This program simulates the damage profile produced by energetic ions into an amorphous target. The program assumes that the target is a perfect solid and does not take into account temperature effects.

The irradiated and the corresponding unirradiated samples were characterized by DB and CDB measurements at room temperature using the variable-energy positron beam at NEPOMUC (FRM II, Garching, Germany) [31,32]. The positron implantation energy varied in the range 1 – 30 keV, which allows obtaining the depth distribution of vacancy-type defects up to ~ 1.2 µm in steel. This would correspond to probe a sample region with a damage of up to ~4 dpa in the single irradiated specimens and ~ 7 dpa in the triple irradiated ones, as calculated from the damage profiles shown in Fig. 1. It has to be noted that the calculated He and H distributions are located far from the studied depth range, although diffusion effects occurring at 600 ºC may significantly broaden the implantation widths.

The Doppler spectrometer allows us to record the annihilation photo-peak at different positron implantation energies up to 30 keV [33]. The positron beam diameter and the beam intensity at the sample were fixed using a 2 mm aperture. The single count rate of the Ge-detectors was about 2500 s^{-1} in the 511 keV photo peak, yielding 1.5 million counts in the annihilation photo-peak after 10 min. The coincident count rate in the photo-peak amounted

to 300 s^{-1}; the total coincident counts in the photo-peak were about 10 million. The Doppler energy shift is $\Delta E = |E_\gamma - 511\ keV|$, where *Eγ* is the energy of the detected annihilation photon, which is related to the component of the electron-positron momentum component along the photon direction p_L by the relation $p_L = 2\Delta E/c$ [34]. The DB spectra of the annihilation peak are recorded as a function of the positron implantation energy. The broadening was characterized using the S and W line shape parameters. The S parameter is calculated as the ratio of counts in the central area of the annihilation peak and the total peak counts. The central area was selected within the energy window of 1.632 keV centered at 511 keV. The W parameter is calculated as the fraction of counts in the high-momentum region corresponding to the energy interval 514.26 – 515.9 keV.

In addition, CDB spectra were recorded in the bulk at incident positron energy of 30 keV. The tail of the 511 keV annihilation peak contains counts related to the positron annihilation events with core electrons. As these electrons also maintain their characteristic energies in solid state, the signal from positron-core electron annihilation can be used to obtain information on the chemical species surrounding the annihilation site [21, 35]. The CDB measurements were carried out using two HP Ge detectors in coincidence, placed face to face and separated by 50 cm with the sample centered between the detectors. In order to compare the CDB measurements, the spectra are normalized and the intensity at a given photon energy is divided by the corresponding counts in the CDB spectrum of a reference sample. Pure annealed Fe and Cr were used as reference samples.

3. Results and discussion

3.1 Single irradiation at room temperature. Fe12Cr and ODS12Cr alloys.

Fig. 2 displays the S and W parameters as a function of incident positron energy for the Fe12Cr and ODS12Cr alloys Fe^{4+} irradiated at room temperature, along with results for

reference samples of unirradiated ODS12Cr and pure annealed Fe. The figure also shows the corresponding mean stopping depth of the positrons in the sample, calculated by [35]

$$\bar{x} = \frac{A}{\rho} E^n \qquad (1)$$

where $A = 4\times10^{-5}$ kg/m^{2}keV$^{1.6}$ and n = 1.6 are empirical parameters, and ρ is the material density.

The S parameter values for incident energies E< 5 keV are governed by the back diffusion of implanted positrons and their annihilation either in a surface state or from a bound electron-positron pair (i.e. positronium) remitted from the sample surface. The back diffusion and formation probability of these states will depend on the positron trapping in the bulk and the surface conditions. The different trend of the S values for E< 5 keV as shown in Fig. 2 for the different samples is attributed to defects in the near surface region due to polishing and contamination of the surface by foreign atoms leading to different surface S parameter. In addition, annihilation of epithermal positrons affects the S-parameter particularly at low energy. However, these effects are not relevant for the further discussion that is focused on the data for E> 5 keV.

The S values for the unirradiated ODS12Cr sample after a slight decreasing trend remain essentially constant for positron energies above ~20 keV indicating a depth-independent positron trapping, i.e. a uniform distribution of positron traps in the bulk. These S values are higher than those obtained for pure annealed Fe, indicating that vacancy-type defects are already present in the unirradiated material. The presence of open volume defects in materials processed by mechanical alloying has already been confirmed by PAS [23]. The increase (decrease) of the S parameter (W parameter) with increasing positron energy is obvious for the Fe^{4+} irradiated Fe12Cr and ODS12Cr samples and is attributed to a higher fraction of

trapped positrons. The above results are consistent with the trend of the calculated displacement-damage profile for these samples shown in Fig. 1.

The CDB spectra of the 12Cr alloys and pure Cr, measured at 30 keV positron energy normalized to the one for annealed pure Fe, are shown in Fig. 3. The ratio curve of pure Cr shows a local minimum at ~$19\times10^{-3}m_oc$. The 12Cr alloys also exhibit this local minimum, which is less pronounced in the irradiated materials compared with the unirradiated ODS12Cr alloy. In addition, the CDB curves for the irradiated 12Cr samples are closer to the one for pure Cr and show a higher fraction of positrons annihilating with low-momentum electrons, i.e. $p_L<3\times10^{-3}m_oc$. The above indicates that the 10 MeV Fe^{4+} irradiation at RT produced a significant concentration of vacancy-type defects at depths up to ~1.2 μm. These defects might have Cr atoms as first neighbors since Fe vacancies and interstitials in bcc Fe and Fe-Cr alloys are both mobile at temperatures above ~220 K [36, 37], and the binding energy of a Fe vacancy-Cr pair is expected to be very small to retain single vacancies trapped by Cr atoms [38]. Thus, the result is interpreted as experimental evidence for the generation of vacancy cluster-Cr complexes under irradiation in the present conditions. The irradiated Fe12Cr and ODS12Cr samples exhibit similar ratio curves to pure Fe as Fig. 3 shows suggesting that the structure of these complex defects would be similar, irrespective of the Y_2O_3 content.

Fig. 4 shows the CDB ratio curves relative to the irradiated Fe12Cr sample. An enhancement of positron annihilations with electrons having momenta in the interval $5\times10^{-3}m_oc<p_L<12\times10^{-3}m_oc$ appears for the irradiated ODS sample, although the values remain lower than those for pure Cr. This enhancement is coincident with the peak attributable to annihilations with core electrons of Cr atoms. It should be noted that the presence of Cr_2O_3 particles is common for both ODS12Cr and Fe12Cr alloys. The required oxygen to form these particles would be provided from the starting elemental powders, which

contain ~ 1.3 at.% O, as well as from the Y_2O_3 powders in the case of the ODS alloy [28]. Moreover, TEM and atom probe tomography studies performed on this ODS12Cr alloy have revealed that the yttrium oxide nanoparticles have either Cr shells or a homogeneous Y-Cr-O composition [28]. The decrease of annihilation events relative to pure Cr in $5\times10^{-3}m_oc<p_L<12\times10^{-3}m_oc$ for the irradiated ODS12Cr and irradiated Fe12Cr alloys (see Fig. 4) might be due to annihilations with core electrons of O atoms, if O atoms were in the surroundings of the positron trapping site. If this effect was due to annihilations with electrons of Y atoms, it would also be expected in the annihilation characteristics of the unirradiated ODS12Cr alloy, but this is obviously not the case. Thus, it appears that the irradiation-induced defects are vacancy cluster-Cr-O complexes.

The correlation between the S and W parameters at incident positron energies > 5 keV is shown in fig. 5. The lines connecting the points in this plot indicate the sequence in which the S and W values were measured with increasing incident positron energy. The presence of the Y-rich nanoparticles in the ODS12Cr alloy actually does not produce any relevant change in the structure of the complex defects induced by the irradiation since the defect-specific S/W ratio [39] for both irradiated samples reflects a similar trend with increasing positron energy.

3.2 Simultaneous triple irradiation at 600ºC. ODS14Cr and ODS14CrWTi alloys.

It has been previously reported that the characteristics of the nanoparticle dispersion in these specific materials as well as their general microstructure differ by virtue of the Ti addition. Y-rich nanoparticles with sizes < 30 nm exhibited either Y-O or Y-Cr-O compositions in the ODS14Cr alloy, and Y-Ti-O compositions in the ODS14CrWTi alloy [29]. In addition to these (Y-Ti)-rich particles, another dispersion of (Cr, Ti)-rich spherical particles with sizes between 50 – 500 nm were also found in the ODS14CrWTi alloy [29]. The presence of

vacancy clusters in the unirradiated alloys that survive annealing at 1400 ºC has been confirmed by PAS lifetime measurements [40].

Fig. 6 depicts the S and W parameters as a function of incident positron energy for the alloys simultaneously irradiated with Fe, He and H ions at 600°C, together with the values for the unirradiated samples. Two irradiated samples of each type were measured, marked as A and B for the ODS14Cr alloy, and C and D for the ODS14CrWTi alloy. The S values measured in the irradiated alloys for positron energies > 5 keV remain smaller than the ones for unirradiated samples, being this effect more noticeable for the ODS14CrWTi alloys, see figure 6b, but in any case higher than the values corresponding to well annealed Fe. This result suggests that the triple irradiation under the present conditions has induced recovery or a change in the characteristics – such as number of vacancies, chemical surrounding or local electron density – of the positron traps. In particular, one feasible explanation that would change the local electron density would be the development of gas bubbles. During the triple beam irradiation at 600 ºC, interstitial atoms and vacancies produced by atom displacements either recombine themselves or sink into the defects already present in the alloys. Simultaneously, the implanted H^+ and He^+ ions, in particular H^+ ions as the most similar particles to positrons, will be trapped in the preexistent defects giving rise to small gas bubbles and increasing the local electron density in the trap. This change in the traps would induce a decrease in the S parameter (as shown in Figs. 6a and b) but no change would be expected in the W parameter (see Figs. 6c and d) as the annihilation events with core electrons from Cr and Fe would not be affected.

Moreover, the S parameter appears to be essentially positron energy independent for energies higher than ~ 5 keV, in contrast to the results for 12Cr alloys after the single irradiation at RT. These results imply that the concentration of vacancy-type defects would remain uniform through the depth range sampled above 5 keV, or there exists saturation trapping of positrons.

Fig. 7 shows the CDB ratio curves with respect to Fe for the irradiated and unirradiated alloys and annealed Cr measured at incident positron energy of 30 keV. The local minimum enhancement at ~$19\times10^{-3} m_o c$ for the irradiated ODS14Cr alloy relative to the unirradiated counterpart indicates the formation of vacancy cluster-Cr defects alike to those induced by the single beam irradiation in the 12Cr alloys. Although this minimum is also evident for the two irradiated ODS14CrWTi samples their ratio curves exhibit characteristics qualitatively different to the corresponding irradiated ODS14Cr samples. The CDB ratio curve for either irradiated ODS14CrWTi samples lies above the one for the unirradiated counterpart sample. This is evidence for less positron traps (defects) after irradiation in opposition to that observed for ODS14Cr (also shown in Fig. 6). Furthermore, the CDB curve for the unirradiated ODS14CrWTi alloy evidences higher content of vacancy defects than in the ODS14Cr unirradiated and irradiated samples, see Fig. 6 and low momentum region in Fig 7. Several studies point out that the alloying element Ti, rather than W, leads to an increase on the number density of nano-features in ODS steels [41]. This would lead to an increase in vacancy type defects, according to experimental and theoretical evidence that would explain the higher vacancy content in the unirradiated ODS14CrWTi sample [42-44]. Moreover, the higher damage recovery in the ODS14CrWTi alloy during irradiation at 600 ºC can be due to the enhanced self-healing of the irradiation damage induced by these nano-features [45, 46].

To highlight the changes induced by the triple irradiation in both alloys, the CDB curves with respect to the corresponding unirradiated samples are depicted in Fig. 8. The probability of positron annihilation with low-momentum electrons, $p_L<5\times10^{-3} m_o c$, in the irradiated ODS14Cr samples is comparable to that for the unirradiated sample (see Fig. 8a), while the annihilation probabilities with electrons of higher momentum, which oscillate around 1, appear to be controlled by core electrons of Fe and Cr atoms. In contrast the annihilation probability with low-momentum electrons is visibly lower for the irradiated ODS14CrWTi

alloy than for its unirradiated counterpart, and significantly higher for electrons with $p_L > 5\times10^{-3} m_o c$, in agreement with the previous explanation (see Fig 8b). Moreover, the minimum due to annihilations with Cr electrons is also evident.

The correlation between the S and W parameters shown in Fig. 9a reveals that the S and W values for the ODS14Cr alloy show no systematic change for positron energies above 5 keV, which indicates only minor changes in the open-volume and chemical surrounding of the defects upon irradiation as well as in their number density. In contrast, the set of S-W data for the irradiated ODS14CrWTi samples shown in Fig. 9b exhibit S values significantly lower than the one for the unirradiated samples, while the W values for irradiated and unirradiated samples lie inside a common interval. This again shows that there are no significant changes in the annihilation events with core electrons from Cr, but there is a decrease on the S parameter because of defect recovery. The W value interval also coincides with that for the ODS14Cr samples (Figs. 9a and 9b). A qualitative change in the W values may not be expected because more than one than one type of defects i.e. at least three competitive positrons traps could be operative in all 14Cr samples. These positron traps would be for instance vacancy cluster-Cr defects, He/H_2 bubbles or defective Y-rich nanoparticles. Future positron lifetime experiments would help to clarify this point.

3.3. Comparison between 12Cr and 14Cr alloys

The single-beam irradiation at RT produces vacancy-type defects in the Fe12Cr and ODS12Cr alloys as the S and W parameters versus positron energy curves reveal (Fig. 2), in contrast with the results obtained from the triple-beam irradiation at 600 ºC for the 14Cr alloys (Fig. 6). Irrespective of the irradiation, the CDB ratio curves for the ODS12Cr and ODS14Cr alloys evidence an increase in the concentration of vacancy-type defects with Cr atoms as nearest neighbors (see Figs. 3 and 7). The fact that both the irradiated Fe12Cr and

ODS12Cr alloys exhibit the same Cr characteristic local minimum supports the above interpretation in opposition to other previous studies attributing this signature to Y-rich oxides [24]. It should be noted that Cr oxides, being more abundant in these alloys, also would yield the same feature in the CDB curve.

4. Conclusions

Fe12Cr alloys

The 10 MeV Fe^{4+} irradiation of the ODS12Cr alloy and its non-ODS counterpart at RT induces effective displacement damage detected by slow positron experiments in a depth range between ~0.15 and 1.2 µm. The CDB spectra acquired at incident positron energy of 30 keV reveal that defects induced by this irradiation in the ODS12Cr and non-ODS Fe12Cr alloys appear to have the same structural characteristics with Cr atoms as nearest neighbors. Defects with similar characteristics were also present in the unirradiated non-ODS alloy, which was produced by the same powder metallurgy route. The CDB ratio curves with respect to the irradiated non-ODS alloy point out to vacancy cluster-Cr-O complexes as defects induced by the Fe^{4+} irradiation under the present conditions.

ODS14Cr and ODS14CrWTi alloys

The S parameter curves for either of the alloys before and after simultaneous (Fe^{5+}+He^{+}+H^{+}) irradiation at 600 ºC are depth independent at incident positron energies >5 keV, and the S values are slightly lower than the corresponding values for the unirradiated alloy. This evidences the presence of a homogeneous concentration of positron traps and the recovery of the irradiation-induced defects by effect of the high irradiation temperature, or transformation of the preexistent defects during the triple beam irradiation at this temperature, for instance the development of gas bubbles induced by trapping of H^{+} and He^{+} at the preexistent vacancy

clusters. In addition, for the ODS14CrWTi alloys the presence of a high density of nano-features would enhance irradiation damage recovery.

The CDB spectra of the irradiated ODS14Cr samples normalized to the corresponding unirradiated sample indicate that these new vacancy clusters induced by the irradiation are associated with Cr atoms as it occurs for the preexistent vacancy clusters in the unirradiated samples.

Acknowledgements

This investigation was supported by the Ministerio de Ciencia e Innovación (Contract ENE2010-17462), and the European Commission through the European Fusion Development Agreement (contract No 09-240) and 7th FP through the "Research infrastructures" action of the "Capacities" Program, NMI3-II (Grant 283883). The authors acknowledge the JANNUS-Saclay team for their scientific and technological advice.

References

[1] D. T. Hoelzer, J Bentley, M. A. Sokolov, M. K. Miller, G. R. Odette, M. J. Alinger, J. Nucl. Mater. 367-370 (2007) 166–172.

[2] P. Yvon, F. Carré, J. Nucl. Mater. 385 (2009)217–222.

[3] S. J. Zinkle, G. S. Was, Acta Materialia 61 (2013) 735–758.

[4] A. Alamo, M. Horsten, X. Averty, E. I. Materna-Morris, M. Reith, J. C. Brachet, J. Nucl. Mater. 283–287 (2000) 353-357.

[5] R. Lindau, A. Möslang, M. Schirra, Fus.Eng. Des. 61-62 (2002) 659- 664.

[6] M. Matijasevic, E. Lucon, A. Almazouzi, J. Nucl. Mater. 377 (2008) 101–108.

[7] R. Schäublin, A.Ramar, N. Baluc, V. de Castro, M. A. Monge, T. Leguey, N. Schmid, C. Bonjour,J. Nucl. Mater. 351 (2006) 247-260.

[8] N. Baluc, J. L. Boutard, S. L. Dudarev, M. Rieth, J. Brito Correia, B. Fournier, J. Henry, F. Legendre,T. Leguey, M. Lewandowska, R. Lindau, E. Marquis, A. Muñoz, B. Radiguet, Z. Oksiuta, J. Nucl. Mater. 417 (2011) 149–153.

[9] A. Kimura, R. Kasada, A. Kohyama, H. Tanigawa, T. Hirose, K. Shiba, S. Jitsukawa, S. Ohtsuka, S. Ukai, M. A. Sokolov, R. L. Klueh, T. Yamamoto and G. R. Odette, J. Nucl. Mater. 367–370 (2007) 60–67.

[10] M. H. Mathon, Y. de Carlan, G. Geoffroy, X. Averty, A. Alamo, C.H. de Novion, J. Nucl. Mater. 312 (2003) 236–248.

[11] R. E. Stoller, (2012). 1.11–Primary radiation damage formation. Comprehensive Nuclear Materials, Elsevier, Oxford, 293-332.

[12] R. L. Klueh, R. L., D. R. Harries. D. R. (2001) High-Chromium Ferritic and Martensitic Steels for Nuclear Applications, ASTM, West Conshohocken, US.

[13] S. J. Zinkle, A. Möslang, Fus.Eng.Des. 88 (2013) 472–482.

[14] G. Brauer, L. Liszkay, B. Molnar, R. Krause, Nucl. Eng. Design 127 (1991) 47-68.

[15] R. Pareja, N. de Diego, R. M. de la Cruz, J. del Río, Nucl. Tech. 104 (1993) 52-63.

[16] V. Slugen, D. Segers, P. M. A. de Bakker, E. de Grave, V. Magula, T. van Hoecke, B. Van Waeyenberge, J. Nucl. Mater. 274 (1999) 273-286.

[17] R. M. Hengstler-Eger, P. Baldo, L. Beck, J. Dorner, K. Ertl, P. B. Hoffmann, C. Hugenschmidt, M. A. Kirk, W. Petry, P. Pikart, and A. Rempel, J. Nucl. Mat. 423 (2012) 170–182.

[18] K. G. Lynn, D. M. Chen, B, Nielsen, R. Pareja, S. Myers, Phys. Rev. B 34 (1986) 1449-1458.

[19] P. J. Schultz, K. G. Lynn, Rev. Mod. Phys. 60 (1988): 701-779.

[20] M. Stadlbauer, C. Hugenschmidt, K. Schreckenbach, and P. Böni, Phys. Rev. B76 (2007) 174104.

[21] P. Asoka-Kumar, M. Alatalo, V.J. Ghosh, A.C. Kruseman, B. Nielsen, K.G. Lynn, Phys. Rev. Lett. 77 (1996) 2097–2100.

[22] P. Pikart, C. Hugenschmidt, J. Mayer, M. Stadlbauer, K. Schreckenbach, Applied Surface Science 255 (2008) 245-247.

[23] Y. Ortega, V. de Castro, M. A. Monge, A. Muñoz, T. Leguey, R. Pareja, J. Nucl. Mater. 376 (2008) 222–228.

[24] M. J. Alinger, S. C. Glade, B. D. Wirth, G. R. Odette, T. Toyama, Y. Nagai, M. Hasegawa, Mater. Sci. Eng. A 518 (2009) 150–157.

[25] R. Kögler, W. Anwand , A. Richter , M. Butterling , Xin Ou , A. Wagner , C.-L. Chen, J. Nucl. Mater. 427 (2012) 133–139.

[26] J. Simeg Veternikova, V. Slugen , S. Sojak , M. Skarba , E. Korhonen , S. Stancek , J. Degmova ,V. Sabelova , I. Bartosova, J. Nucl. Mater. 450 (2014) 99-103.

[27] J. Simeg Veterníková, J. Degmová, V. Sabelová, M. Petriska,V. Slugeň, Appl. Surf. Sci. 312 (2014) 199-202.

[28] V. de Castro, E. A.Marquis, S. Lozano-Perez, R. Pareja, M. L. Jenkins, Acta Mater. 59 (2011) 3927-3936.

[29] M.A. Auger, V. de Castro, T. Leguey, M.A. Monge, A. Muñoz, R. Pareja, J. Nucl. Mater. 442 (2013) S142-S147.

[30] J. F. Ziegler, M. D. Ziegler, J. P. Biersack, J. P. Nucl.Instrum. Meth. B268 (2010) 1818-1823.

[31] C. Hugenschmidt, G. Kögel, R. Repper, K. Schreckenbach, P. Sperr, B. Straßer, W. Triftshäuser, Nucl. Instrum.Meth. B 221 (2004) 160–164.

[32] C. Hugenschmidt, H. Ceeh, T. Gigl, F. Lippert, C. Piochacz, M. Reiner, K. Schreckenbach, S. Vohburger, J. Weber, and S. Zimnik, J. Phys. Conf. Ser. 505 (2014) 012029.

[33] M. Stadlbauer, C. Hugenschmidt, K. Schreckenbach, Appl. Surf. Sci. 255 (2008) 136–138.

[34] R. S. Brusa, S. Mariazzi, L. Ravelli, P. Mazzoldi, G. Mattei, W. Egger, C. Hugenschmidtd, B. Löwed, P. Pikartd, C. Macchie, A. Somoza, Nucl. Instrum. Meth. B 268 (2010) 3186-3190.

[35] A. Vehanen, K. Saarinen, P. Hautojärvi, H. Huomo, Phys. Rev. B. 35 (1987) 4606 – 4610.

[36] A. Vehanen, P. Hautojarvi, J. Johansson, J. Yli-Kauppila, Phys. Rev. B 25 (1982) 762 – 780.

[37] C.Dimitrov, A. Benkaddour, C. Corbel, P. Moser, Ann. Chim. Fr. 16 (1991) 319 – 324.

[38] P. Olsson, T. P. C Klaver, C. Domain, Phys. Rev. B 81 (2010) 054102.

[39] S. Mantl, W. Triftshaüser, Phys. Rev B 17 (1978) 1645 – 1652.

[40] R. Dominguez, M.A. Auger, M.A. Monge, R. Pareja, submitted.

[41] J. L. Boutard, A. Alamo, R. Lindau, M. Rieth, C. R. Phys. 9 (2008) 287–302.

[42] C. L. Fu, M. Krčmar, G. S. Painter, X-Q. Chen, Phys. Rev. Lett. 99 (2007) 225502 (1-4).

[43] J. Xu, C. T. Liu, M. K. Miller, H. Chen, Phys. Rev. B 79 (2009) 20204 (1-4).

[44] A. Hirata, T. Fujita, H. R. Wen, J. H. Scheibel, C. T. Liu, M. W. Chen, Nature Mater. 10 (2011) 922-926.

[45] T. Yamamoto, G. R. Odette, T. Miao, D. T. Hoelzer, J. Bentley, N. Hashimoto, H. Tanigawa, R. J. Kurtz, J. Nucl. Mater. 367-370 (2007) 399-410.

[46] G. R. Odette. M. J. Alliger, B. D. Wirth, Annu. Rev. Mater. Res. 38 (2008) 471-503.

Table 1. Composition and irradiation conditions of investigated alloys

Alloy	Composition (wt%)	Irradiation
Fe12Cr	Fe-12Cr	Single
ODS12Cr	Fe-12Cr-0.4Y_2O_3	Single
ODS14Cr	Fe-14Cr-0.3Y_2O_3	Triple
ODS14CrWTi	Fe-14Cr-2W-0.3Ti-0.3Y_2O_3	Triple

One column width

Table 2. Irradiation conditions and calculated dpa for the single and triple irradiations.

Ions	Energy	Temp (ºC)	Dose rate (ions·m^{-2}·s^{-1})	Fluence (ions·m^{-2})	
Single Irradiation					
Fe^{4+}	10 MeV	20	4.60×10^{15}	5.0×10^{19}	~10 dpa
Triple Irradiation					
Ions	Energy	Temp (ºC)	Dose rate (ions·m^{-2}·s^{-1})	Fluence (ions·m^{-2})	
Fe^{5+}	14 MeV	600	8.3×10^{15}	1.49×10^{20}	~ 30 dpa
He^{+}	1.6 MeV		8×10^{14}	1.4×10^{19}	~ 600 appm
H^{+}	500 keV		1.97×10^{15}	3.55×10^{19}	~ 1500 appm

One column width

Figure captions

Fig.1. Profiles of irradiated samples calculated by SRIM. (a) Damage profile of Fe ions in the single-ion irradiation, and (b) damage profile of Fe ions in the triple irradiation and He and H ion implantation profiles.

Fig. 2. (a) S parameter and (b) W parameter for the unirradiated ODS12Cr and irradiated ODS12Cr and Fe12Cr samples as a function of incident positron energy.

Fig. 3. CDB ratio curves to Fe for the unirradiated ODS12Cr sample, the irradiated ODS12Cr and Fe12Cr samples, and reference Cr. The CDB spectra were measured at 30 keV incident positron energy.

Fig. 4. CDB ratio curves to the irradiated Fe12Cr sample for the unirradiated and irradiated ODS12Cr samples, reference Fe and reference Cr. The CDB spectra were measured at 30 keV incident positron energy.

Fig. 5. S–W correlation for the unirradiated ODS12Cr and the irradiated ODS12Cr and Fe12Cr samples measured at incident positron energies in the 6-30 keV range.

Fig. 6. (a) S parameter and (c) W parameter for the unirradiated and irradiated ODS14Cr samples as function of incident positron energy. (b) S parameter and (d) W parameter for the unirradiated and irradiated ODS14CrWTi samples as function of incident positron energy. Two irradiated samples of each type were measured, marked as A and B for the ODS14Cr alloy, and C and D for the ODS14CrWTi alloy. The values for Fe

are shown as reference.

Fig. 7. CDB ratio curves to Fe for the unirradiated and irradiated ODS14Cr and ODS14CrWTi samples and reference Cr. The spectra were measured at incident positron energy of 30 keV.

Fig. 8. (a) CDB ratio curves to the unirradiated ODS14Cr alloy for reference Fe, reference Cr and the irradiated ODS14Cr samples. (b) CDB ratio curves to the unirradiated ODS14Cr alloy for reference Fe, reference Cr, and the irradiated ODS14CrWTi samples.

Fig. 9. S–W correlation for (a) the unirradiated ODS14Cr and irradiated ODS14Cr samples and (b) the unirradiated ODS14CrWTi and irradiated Fe14CrWTi samples measured at incident positron energies in the 6-30 keV range.

Figure 1
Click here to download high resolution image

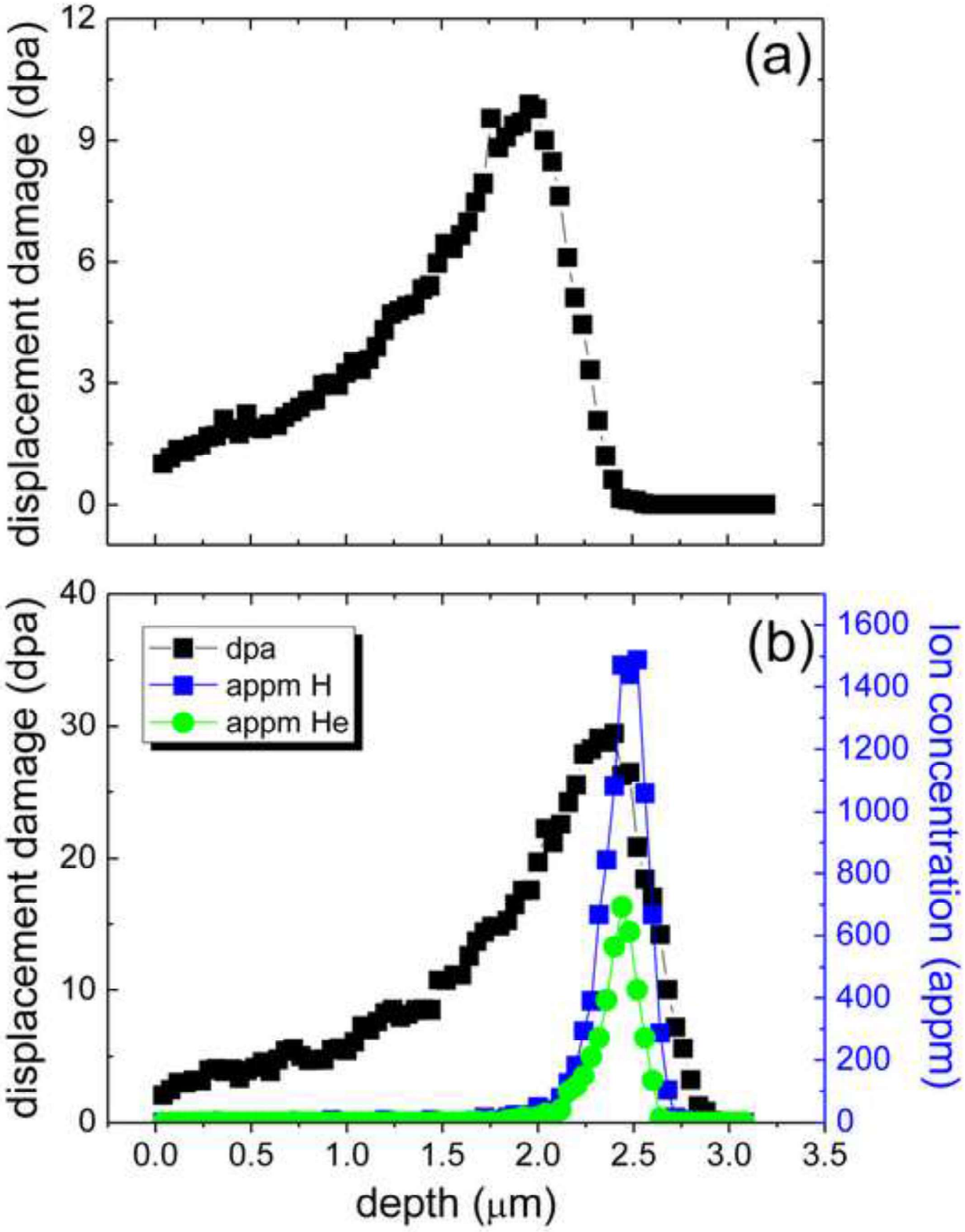

Figure 2
Click here to download high resolution image

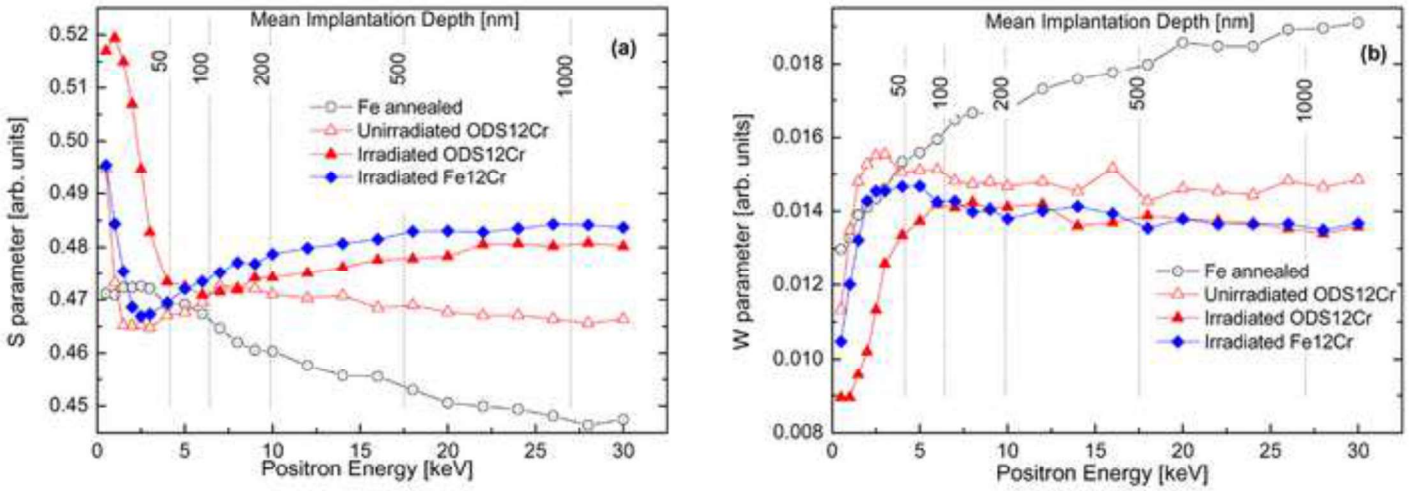

Figure 3
Click here to download high resolution image

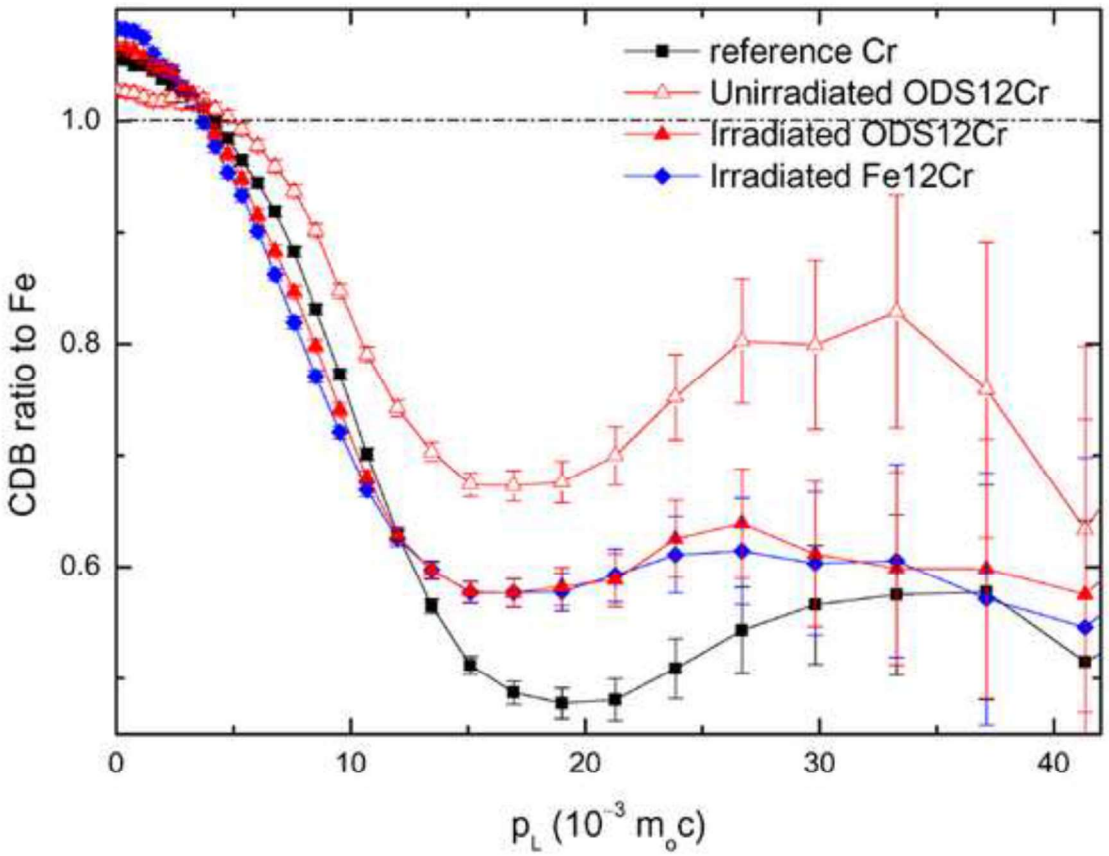

Figure 4
Click here to download high resolution image

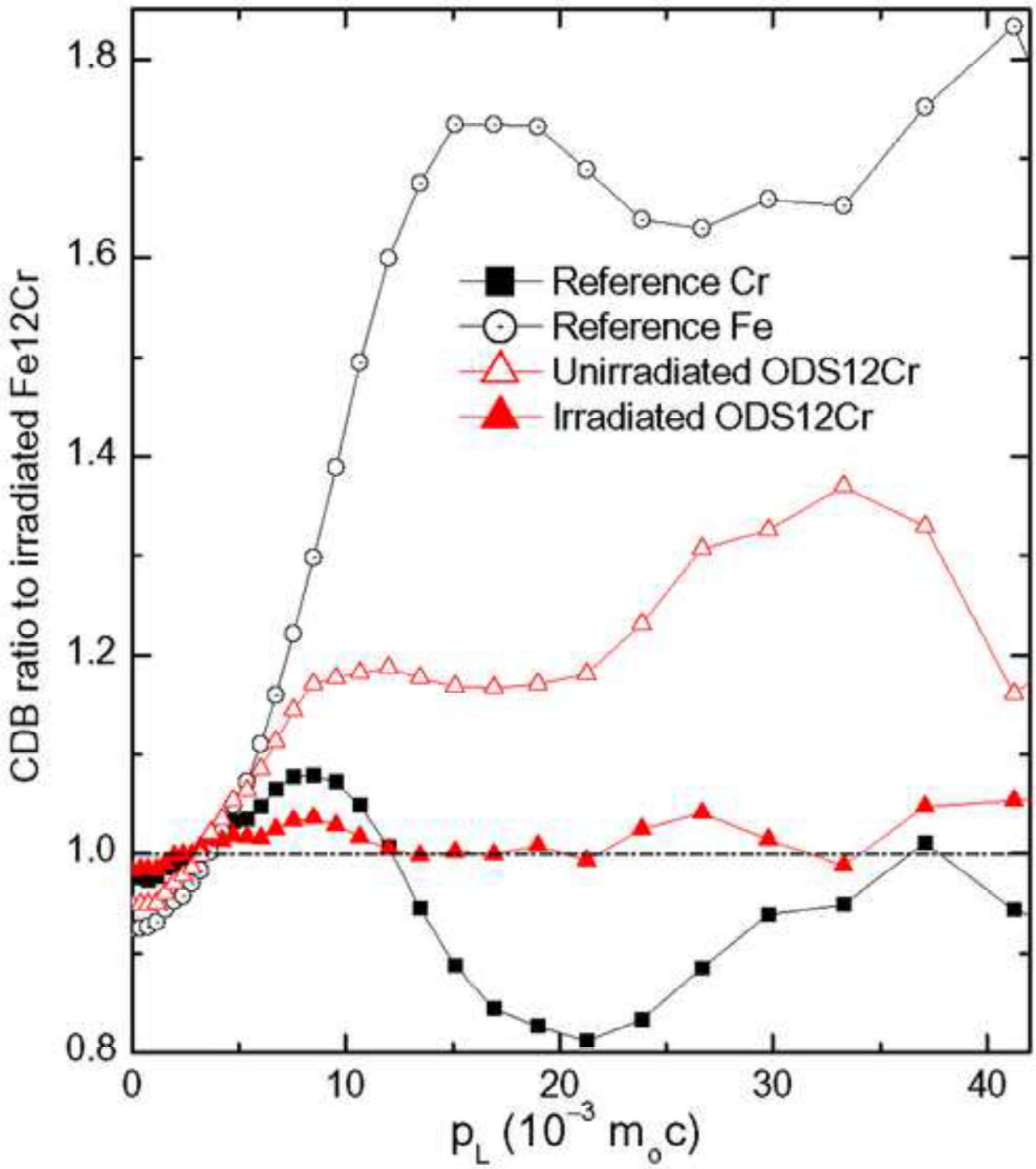

Figure 5
Click here to download high resolution image

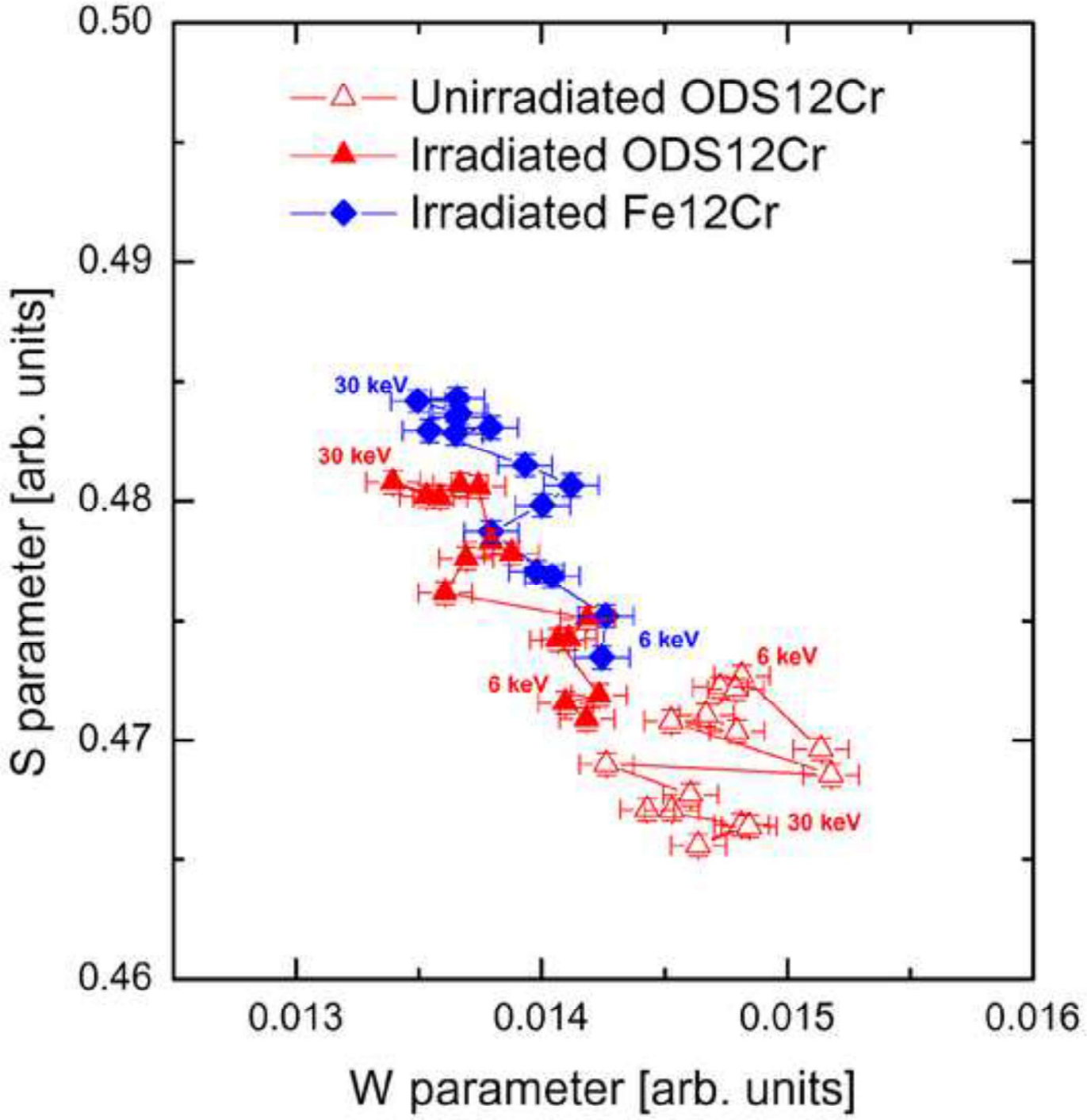

Figure 6
Click here to download high resolution image

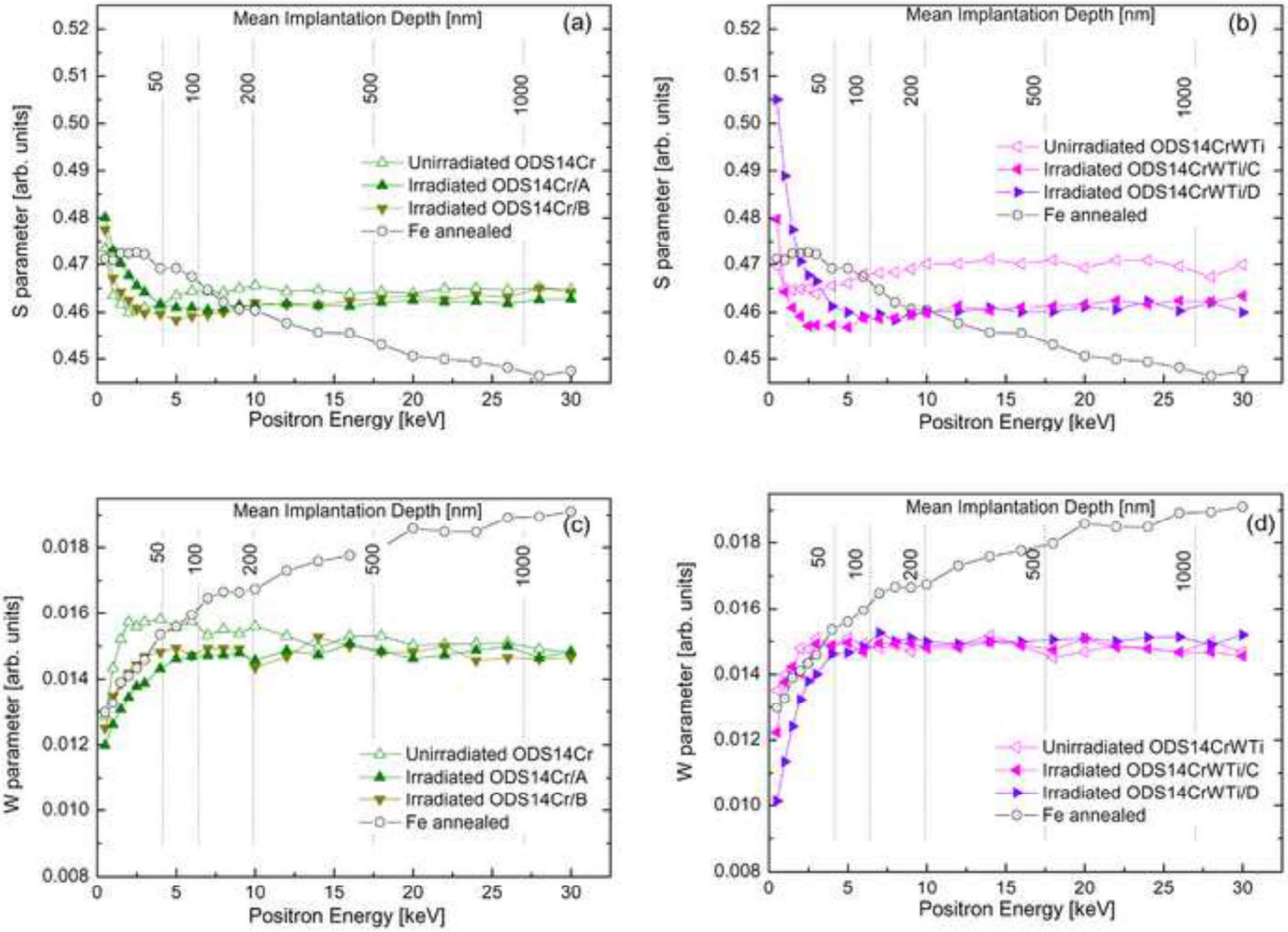

Figure 7
Click here to download high resolution image

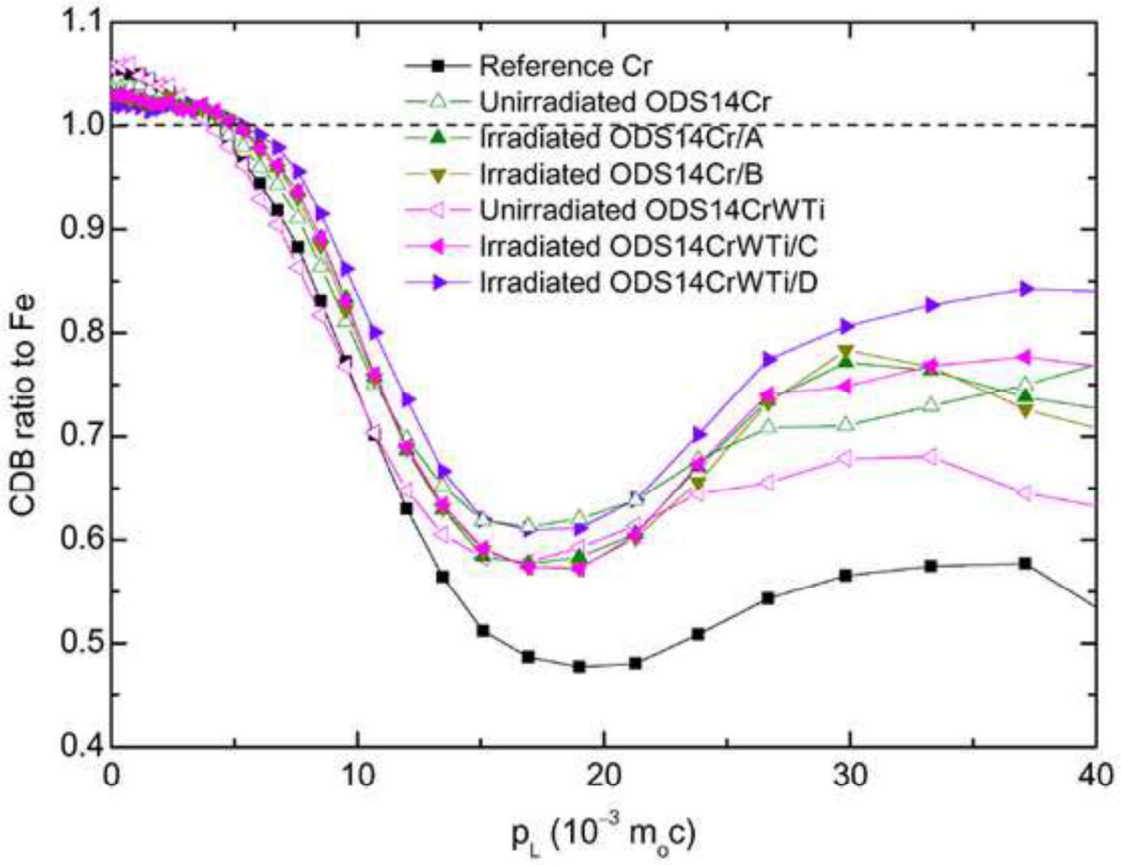

Figure 8
Click here to download high resolution image

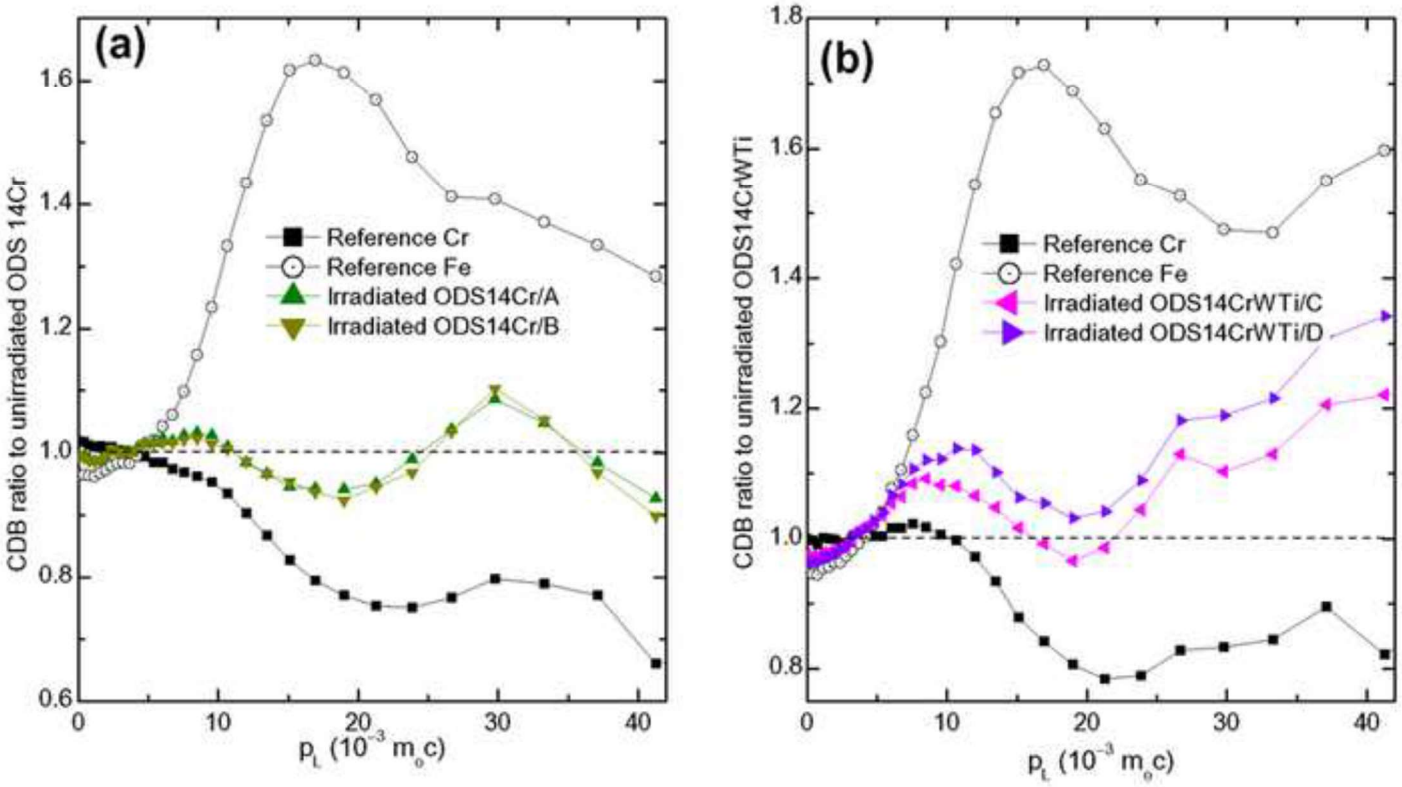

Figure 9
Click here to download high resolution image